JBC ARTICLE

Multiple roles of filopodial dynamics in particle capture and phagocytosis and phenotypes of Cdc42 and Myo10 deletion

Received for publication, November 8, 2016, and in revised form, March 13, 2017 Published, Papers in Press, March 13, 2017, DOI 10.1074/jbc.M116.766923

Markus Horsthemke[‡], Anne C. Bachg[‡], Katharina Groll[‡], Sven Moyzio[‡], Barbara Müther[‡], Sandra A. Hemkemeyer[‡], Roland Wedlich-Söldner[§], Michael Sixt[¶], Sebastian Tacke[‖], Martin Bähler[‡], and Peter J. Hanley[‡1]

From the [‡]Institut für Molekulare Zellbiologie, Westfälische Wilhelms-Universität Münster, 48149 Münster, Germany, the [§]Institut für Zelldynamik und Bildgebung, Westfälische Wilhelms-Universität Münster, 48149 Münster, Germany, the [¶]Institute of Science and Technology Austria (IST Austria), Klosterneuburg, Austria, and the [‖]Institut für Medizinische Physik und Biophysik, Westfälische Wilhelms-Universität Münster, 48149 Münster, Germany

Edited by Velia M. Fowler

Macrophage filopodia, finger-like membrane protrusions, were first implicated in phagocytosis more than 100 years ago, but little is still known about the involvement of these actin-dependent structures in particle clearance. Using spinning disk confocal microscopy to image filopodial dynamics in mouse resident Lifeact-EGFP macrophages, we show that filopodia, or filopodia-like structures, support pathogen clearance by multiple means. Filopodia supported the phagocytic uptake of bacterial (*Escherichia coli*) particles by (i) capturing along the filopodial shaft and surfing toward the cell body, the most common mode of capture; (ii) capturing via the tip followed by retraction; (iii) combinations of surfing and retraction; or (iv) sweeping actions. In addition, filopodia supported the uptake of zymosan (*Saccharomyces cerevisiae*) particles by (i) providing fixation, (ii) capturing at the tip and filopodia-guided actin anterograde flow with phagocytic cup formation, and (iii) the rapid growth of new protrusions. To explore the role of filopodia-inducing Cdc42, we generated myeloid-restricted Cdc42 knock-out mice. Cdc42-deficient macrophages exhibited rapid phagocytic cup kinetics, but reduced particle clearance, which could be explained by the marked rounded-up morphology of these cells. Macrophages lacking Myo10, thought to act downstream of Cdc42, had normal morphology, motility, and phagocytic cup formation, but displayed markedly reduced filopodia formation. In conclusion, live-cell imaging revealed multiple mechanisms involving macrophage filopodia in particle capture and engulfment. Cdc42 is not critical for filopodia or phagocytic cup formation, but plays a key role in driving macrophage lamellipodial spreading.

Phagocytosis is a specialized form of endocytosis, which requires localized actin polymerization to engulf large particles ($> \sim 0.5\ \mu m$), and initially involves particle binding to phagocytic receptors, which triggers phagocytic cup formation through the activation of kinases, such as Syk, and Rho GTPases, such as the Cdc42 and Rac subfamilies (1). Although phagocytosis has been investigated in-depth, the involvement of filopodia (finger-like projections containing bundled actin filaments (2)) in actually capturing and clearing particles has not been conclusively demonstrated, except for the historical observations of Metschnikoff (3) and more recent work using brightfield microscopy (4–7).

Young *et al.* (4) observed using time-lapse differential interference contrast (DIC)[2] imaging that *Escherichia coli* expressing invasin, a transmembrane protein of *Yersinia pseudotuberculosis*, could enter Hep-2 (HeLa-derived) cells via filopodia. Using another approach, coating of magnetic microbeads with invasin, Vonna *et al.* (5) found that the adhesion of beads to filopodial tips induced pulling toward the cell body. Similarly, Kress *et al.* (6) reported that filopodia act as "phagocytic tentacles" and pulled IgG-coated beads in an optical trap with discrete steps, suggesting that a motor protein was involved. More recently, Möller *et al.* (7) reported that macrophages can use filopodia to lift membrane-bound bacteria, thereby enabling a lamellipodial protrusion to engulf the target in a so-called hook-and-shovel mechanism.

In this study, we looked at phagocytosis from a new angle. We isolated resident peritoneal macrophages from transgenic Lifeact-EGFP mice (8) and used time-lapse spinning disk confocal microscopy to visualize the involvement of filopodial dynamics in the clearance of fungal and bacterial particles. Lifeact-EGFP mice ubiquitously express the F-actin-binding (17-amino acid) peptide Lifeact fused to the 238-amino acid fluorescent protein EGFP (9). The filopodia-inducing proteins Cdc42 and Myo10 have both been implicated in phagocytosis (10, 11). Using knock-out mouse models, we explored the roles of these proteins in macrophage phagocytosis.

This work was supported by Deutsche Forschungsgemeinschaft Grant HA 3271/4-1 (to P. J. H.) and EXC 1003 (Cluster of Excellence 1003), Cells in Motion (CiM). The authors declare that they have no conflicts of interest with the contents of this article.
This article contains supplemental Videos S1–S9.

[1] To whom correspondence should be addressed. Tel.: 49-251-83-23854; Fax: 49-251-83-24723; E-mail: hanley@uni-muenster.de.

[2] The abbreviations used are: DIC, differential interference contrast; SR-SIM, superresolution-structured illumination microscopy; TLR, Toll-like receptor; MR, mannose receptor; cKO, conditional knock-out; IRES, internal ribosomal entry site; EGFP, enhanced green fluorescent protein.

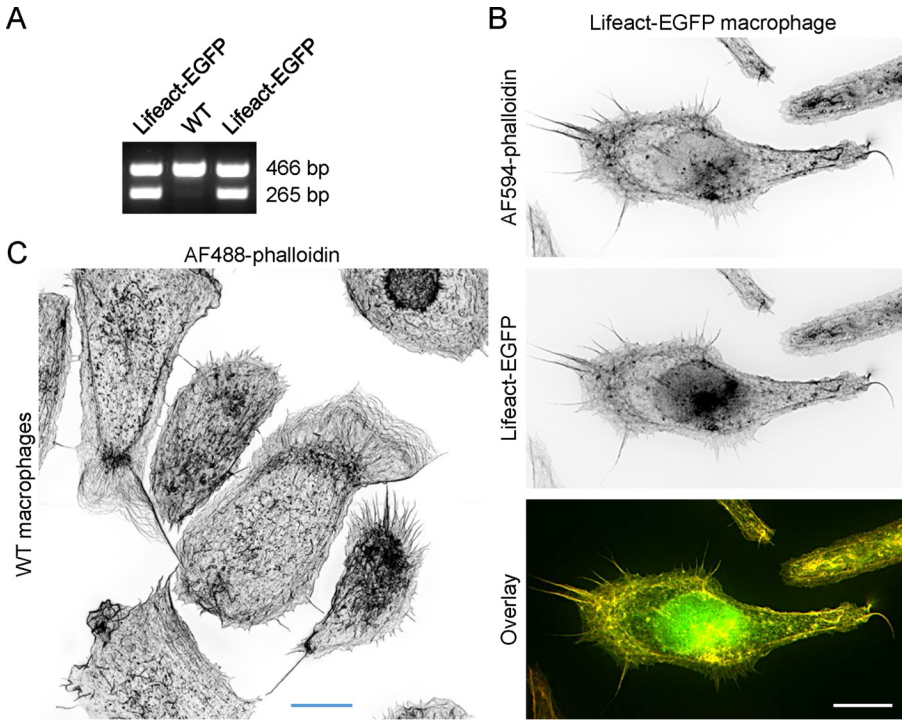

Figure 1. SR-SIM imaging of actin filaments in macrophages. *A*, PCR genotyping of offspring derived from crossing heterozygous Lifeact-EGFP and wild-type (WT) mice. *B*, resident peritoneal macrophage isolated from a Lifeact-EGFP mouse. After fixation and permeabilization, the cell was stained with Alexa Fluor 594 (AF594)-conjugated phalloidin, an F-actin probe, and imaged by SR-SIM. The single channel images have been inverted. *Scale bar*, 10 μm. *C*, SR-SIM (inverse) image of fixed and permeabilized mouse macrophages, stained with Alexa Fluor 488 (AF488)-conjugated phalloidin. The image, obtained via an oil-immersion ×63/NA 1.4 objective lens, is an overlay of 3 *z*-slices taken at 220 nm steps. *Scale bar*, 10 μm.

Results

Capture of zymosan particles by filopodial tentacles

Initially, we used superresolution-structured illumination microscopy (SR-SIM) to confirm that Lifeact-EGFP is expressed in resident peritoneal macrophages and localizes to F-actin (Fig. 1, *A* and *B*). Whereas Lifeact-EGFP and the high-affinity F-actin probe phalloidin, conjugated to Alexa Fluor 594, clearly co-localized, Lifeact-EGFP additionally accumulated in the nucleus. Similar to Lifeact-EGFP, we previously observed that EGFP alone also accumulated in the nuclei of resident peritoneal macrophages (isolated from LysM-EGFP ($Lyz2^{tm1.1Graf}$) mice (12)). SR-SIM imaging provided striking detail of the actin architecture in macrophages (Fig. 1*C*). Instead of a dense branching network, typical for the lamellipodial membrane protrusions of fibroblast-like and epithelial cells (13, 14), SR-SIM imaging showed nicely that macrophage lamellipodial membrane protrusions, as well as the cell body, are rich in arcs of actin bundles orientated parallel to the cell periphery. In addition, we observed that one or more prominent filopodial tentacles, or even a cluster of tentacles, typically extend from the cell periphery.

Using 2-channel spinning disk confocal microscopy, we found that the tips of filopodial tentacles were capable of capturing fluorescent zymosan particles (Fig. 2, *A*–*C*; supplemental Videos S1–S3). Once captured, the tentacle retracted, but concomitantly, it served as a bridge for the flow of actin and membrane toward and around the particle (Fig. 2, *A* and *C*; supplemental Videos S1 and S3). Time-lapse imaging revealed that new filopodial tentacles sprouted at active sites of tentacle-mediated capture and engulfment (Fig. 2, *A*–*C*; supplemental Videos S1–S3). Filopodial extensions could also be observed arising from closed phagocytic cups in snapshots of phagocytic events captured by fixation and scanning electron microscopy (Fig. 2*D*). While performing spinning disk confocal microscopy experiments, we invariably observed dynamic actin "hot spots" within the actin ring (corresponding to the phagocytic cup) surrounding ingested zymosan particles, and we speculated that these spots may correspond to transient filopodial tentacles emerging from the phagocytic cup. Instead, these hot spots, which accompany each uptake event, were variously located beneath, alongside, and above zymosan particles, and presumably serve as local pools of actin.

We assumed that zymosan uptake in our assays was triggered via the recognition of β-glucans by Dectin-1 (15), although both TLRs (Toll-like receptors) (16) and the MR (mannose receptor) (17, 18) have been implicated in zymosan phagocytosis. To assess the contribution of these receptors to zymosan phagocytosis in our assays, we compared the phagocytic activity of wild-type (WT) *versus* Toll-like receptor-2/4 double knock-out (dKO), mannose-receptor knock-out, or Dectin-1 knock-out macrophages. Using zymosan particles labeled with the pH-sensitive dye pHrodo, which becomes brighter at decreasing pH (Fig. 3, *A* and *B*), we could measure phagosome acidification, a readout for particle internalization. One caveat of this approach is that a subset of macrophages exhibits weak phagosome acidification (for example, see Fig. 3*C*). Nevertheless, using this approach, we could confirm that Dectin-1 is the primary recep-

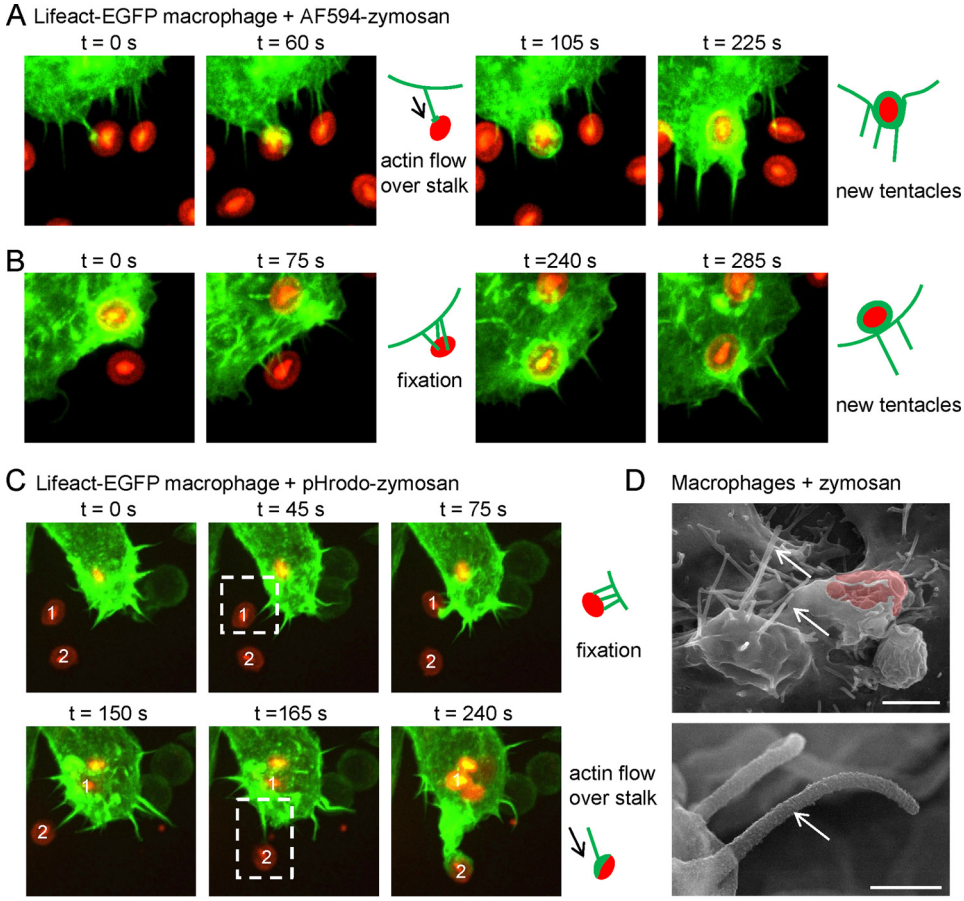

Figure 2. Capture and ingestion of zymosan particles via filopodia extending from mouse resident peritoneal Lifeact-EGFP macrophages. *A*, time-lapse images (20 × 20 μm) showing phagocytic cup formation upon a filopodium, which has captured an Alexa Fluor 594-conjugated zymosan (AF594-zymosan) particle (*red*), followed by the growth of new filopodial tentacles. *B*, time-lapse images (20 × 20 μm) of a zymosan particle being fixed by the extension of short filopodia, followed by engulfment and the formation of new filopodial tentacles. *C*, time-lapse images (25 × 25 μm) showing the capture and ingestion of two pHrodo-labeled zymosan particles (labeled *1* and *2*) via filopodial tentacles. *D*, scanning electron microscopy images of macrophages engulfing zymosan particles. *Top image*: filopodia, indicated by *white arrows*, protruding from a closed phagocytic cup, and a partially enveloped zymosan particle, pseudocolored *red*. *Scale bar*, 2 μm. *Bottom image*: close-up view of a filopodium (indicated by an *arrow*). *Scale bar*, 400 nm.

tor mediating both the binding and internalization of zymosan particles (Fig. 3*D*).

Multiple modes of filopodial tentacles in bacterial particle clearance

Next, we investigated the involvement of filopodial tentacles in the capture of *E. coli* particles (Fig. 4). Time-lapse spinning disk confocal microscopy revealed that filopodial tentacles were highly effective at clearing particles beyond the cell body. Once captured by the tips of filopodia, particles were retracted toward the cell body and internalized, or, alternatively, the sweeping of a tentacle was effective at bringing particles toward the cell body (Fig. 4, *A* and *B*; supplemental Videos S4 and S5). The growth of new filopodial tentacles, fed by a pool of actin, could be observed in time-lapse recordings (Fig. 4*A*; supplemental Video S4). In addition to retraction and sweeping, the surfing of particles along the shaft of filopodial tentacles was frequently observed (Figs. 4*C* and 5, *A* and *B*; supplemental Videos S6–S8). Particles surfed (moved) along filopodia with a velocity of 1–2 μm/min (Fig. 5*C*). Combinations of surfing and retraction were also frequently observed (supplemental Video S9). As illustrated in Fig. 5*D*, surfing and combinations of surfing and retraction accounted for the majority of filopodia-mediated *E. coli* particle uptake events. We speculated that actin retrograde flow may drive the surfing of particles (see "Discussion"). Using kymograph analyses we found that the velocity of actin retrograde flow (treadmilling) in Lifeact-EFGP macrophages was in the range 2–4 μm/min (Fig. 5*E*), consistent with previous reports (19, 20).

Cdc42-deficient macrophages

To investigate the role of Cdc42 in macrophage filopodial tentacle formation and phagocytosis we generated myeloid-restricted Cdc42 (conditional) knock-out (cKO) mice (Fig. 6). Conditional deletion was confirmed by Western blot analysis of lysates from F4/80$^+$ cells (macrophages), purified by cell sorting (Fig. 6*A*). Spinning disk confocal microscopy of living cells (not shown in Fig. 6, but see Fig. 13*D*) and superresolution imaging of fixed cells stained with an F-actin probe, Alexa Fluor 488-conjugated phalloidin, showed that Cdc42-deficient macrophages had a severe cell spreading defect (Fig. 6*B*), reminiscent of Myo9b-deficient macrophages, which have overactive RhoA activity (21). Indeed, Cdc42-deficient macrophages were resistant to cell spreading, even in the presence of the Toll-like receptor 4 ligand lipopolysaccharide (LPS), used to activate cells, as shown in Fig. 6*C* and quantified in Fig. 6*D*,

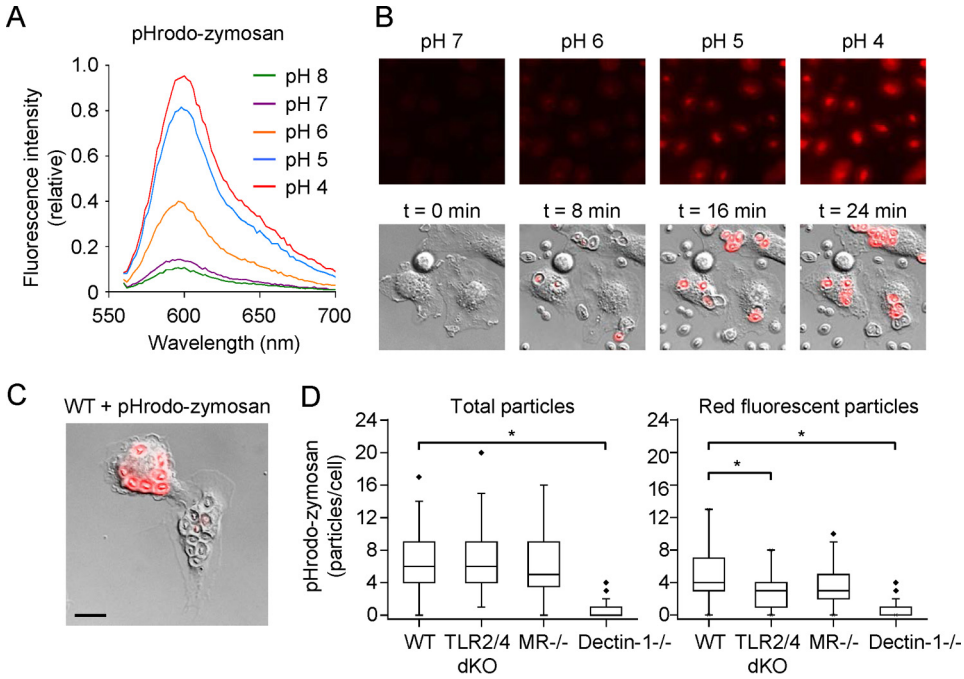

Figure 3. Dectin-1 mediates zymosan binding and internalization. *A*, fluorescence emission spectra of pHrodo-conjugated zymosan particles suspended in buffers with different pH values, ranging from pH 4 to 8. Particles were labeled using the succinimidyl ester of pHrodo. *B*, *top panel*: DIC and fluorescence images of pH-sensitive pHrodo-conjugated zymosan particles superfused with media buffered to different pH values, as indicated. *Bottom panel*: time-lapse images showing the ingestion and acidification of pHrodo-conjugated zymosan particles. *C*, DIC image, with superimposed red fluorescence, of two wild-type (WT) macrophages, which have ingested multiple pHrodo-conjugated zymosan particles. *Red* fluorescence indicates acidification of phagosomes. *Scale bar*, 10 μm. *D*, box plots of the number of attached (*left*) and red fluorescent (*right*) pHrodo-conjugated zymosan particles in WT, Toll-like receptor 2/4 double knock-out (TLR2/4 dKO), mannose receptor knock-out ($MR^{-/-}$), and Dectin-1 knock-out ($Dectin\text{-}1^{-/-}$) macrophages. Cells, seeded in fibronectin-coated μ-slide I chambers, were incubated with particles for 15 min before washing. *, $p < 0.05$; Kruskal-Wallis one-way analysis of variance on ranks (at the 0.05 level of significance).

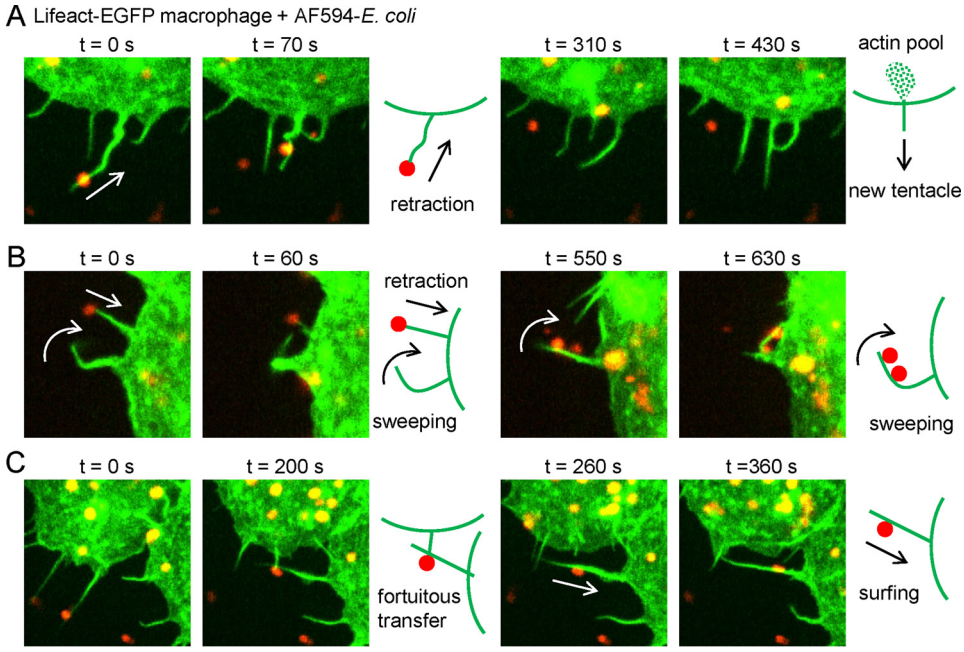

Figure 4. Multiple modes of filopodia-mediated capture and ingestion of bacterial particles. *A*, time-lapse images (15 × 15 μm) showing the capture of an Alexa Fluor 594-conjugated *E. coli* (*AF594-E. coli*) particle (*red*) by a filopodium of a mouse resident peritoneal Lifeact-EGFP macrophage, followed by retraction toward the cell body and the growth of a new filopodial tentacle. *B*, time-lapse images (15 × 15 μm) showing the retraction of a filopodium with an *E. coli* particle on its tip, as well as the clearance of *E. coli* particles by the sweeping action of another filopodial tentacle. *C*, time-lapse images (20 × 20 μm) showing the fortuitous transfer of an *E. coli* particle from the filopodium of one cell to the filopodium of another cell. The particle is pulled toward the cell body by the first filopodium, then, following transfer, it appears to "surf" along the second filopodium.

where the projected cell area is used as an index of spreading. Unstimulated Cdc42 cKO macrophages exhibited less filopodia per cell compared with WT cells (Fig. 6*E*). However, LPS stimulation for 90 min increased the number of filopodia per cell in both WT and Cdc42 cKO cells, such that there was no significance difference between activated (+LPS) WT and Cdc42

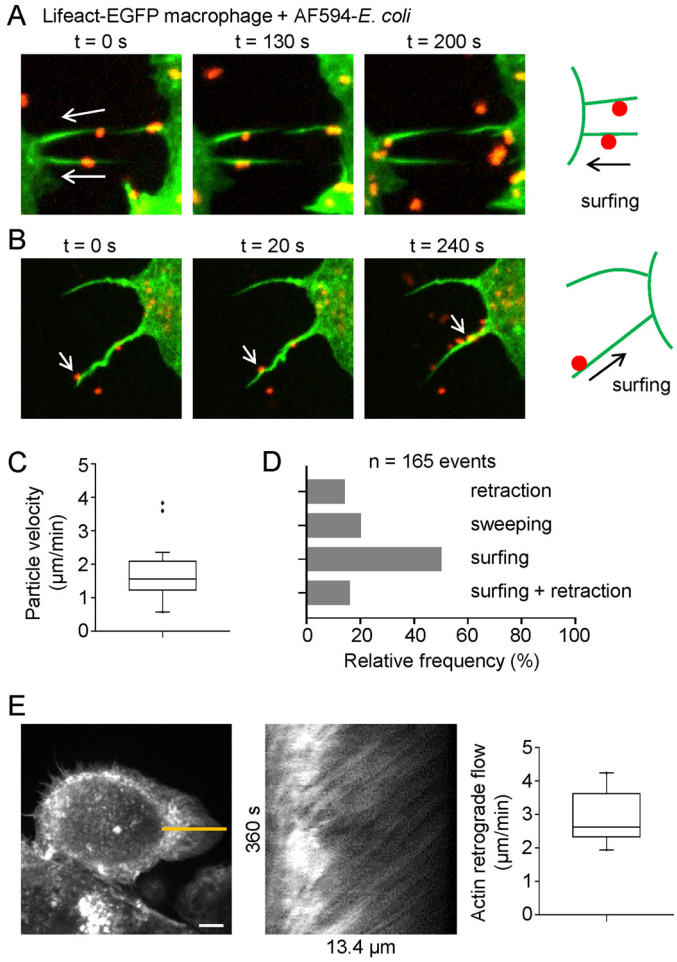

Figure 5. Filopodia-mediated uptake of bacterial particles. *A*, time-lapse images (20 × 20 μm) showing captured *E. coli* particles surfing along filopodia toward the cell body. *B*, another example of *E. coli* particles surfing along a filopodium (images are 20 × 20 μm). *C*, box plot of the velocity of *E. coli* particles surfing along filopodia. *D*, normalized frequency (all events = 100%) of different modes in filopodia-mediated phagocytic events. *E*, measurement of actin retrograde flow in Lifeact-EGFP macrophages by kymograph analysis.

cKO cells (Fig. 6*E*). In addition, the median length of filopodia was shorter in unstimulated Cdc42 cKO macrophages, compared with WT, and LPS stimulation significantly increased filopodia length in both WT and Cdc42 cKO macrophages (Fig. 6*F*). We could not detect the putative filopodia-inducing Rho GTPases RhoJ, RhoQ, RhoD, or RhoF in mouse macrophages using RT-PCR and Western blot analyses (Fig. 7, *A* and *B*). Thus, Cdc42 is presumably the predominant filopodia-inducing Rho GTPase in macrophages (22), and, in Cdc42-deficient cells, the paucity of filopodia, but not cell spreading, is compensated by LPS stimulation.

Using time-lapse spinning disk confocal microscopy and fluorescent labeling of the cell membrane with Alexa Fluor 488-conjugated anti-F4/80 antibodies, we imaged the engulfment of large (diameter, 5.19 μm) mouse IgG-coated polystyrene beads by macrophages (Fig. 8). Most beads were taken up after passive contact with the cell membrane. The kinetics of phagocytic cup formation was measured by tracking XY, XZ, and YZ views of the cells (Fig. 8). Surprisingly, Cdc42-deficient macrophages were highly efficient at engulfing large particles (Fig. 8*A*), and the rate of cup closure was faster compared with WT cells (Fig. 8, *B–D*). However, the start of phagocytic cup formation may have been underestimated in Cdc42-deficient cells due to the highly ruffled surface of these rounded-up cells (Fig. 9*A*). In contrast, the initiation of phagocytic cup formation could be more easily detected in spread-out WT macrophages, especially when particles landed on lamellipodia (Fig. 8*B*). Nevertheless, whether first or second phagocytic half-cup kinetics were measured (Fig. 8*D*), Cdc42 cKO macrophages were faster at enveloping large beads. Notably, we occasionally observed that filopodia could haul in large particles before phagocytic cup formation was initiated (Fig. 9*B*), but these events were excluded from the above analyses in Fig. 8*D*.

Although Cdc42 cKO macrophages had faster phagocytic cup kinetics than WT cells, mutant cells engulfed less IgG-coated polystyrene beads and zymosan particles in end-point assays (Fig. 10*A*), presumably due to less frequent contacts (see "Discussion"). SR-SIM imaging of Cdc42-deficient macrophages, which were fixed while engulfing zymosan particles, revealed filopodia projecting from phagocytic cups (Fig. 10*B*).

Aside from phagocytosis (23), Cdc42 is implicated in chemotactic navigation (24–26). Using real-time chemotaxis assays, we found that Cdc42-deficient macrophages had greatly impaired chemotactic navigation and modestly decreased median cell velocity (Fig. 10, *C* and *D*). Chemotaxis assays were performed in a complement C5a gradient (target concentration, 20 nM) and a uniform concentration of LPS (0.1 μg/ml).

Myo10 is implicated in phagocytosis (11), especially in the engulfment of large particles, and it is thought to act downstream of Cdc42 in the generation of filopodia (27). We confirmed deletion of Myo10 in homozygous Myo10 reporter knock-out ($Myo10^{tm2/tm2}$) mice using Southern and Western blot analyses, as well as PCR analysis (Fig. 11*A*).[3] In contrast to Cdc42-deficient macrophages, Myo10 knock-out macrophages exhibited no defects in cell velocity or chemotactic navigation (Fig. 11*B*). Moreover, there were no impairments in phagocytic cup formation and the ingestion of large particles (Fig. 11, *C–E*). Consistent with the time-lapse imaging data, no differences in the uptake of particles could be detected in end-point assays (Fig. 11*F*). To test whether Myo10-deficient macrophages have impaired filopodia formation we performed dynamic assays because filopodia cannot be unambiguously distinguished from retraction fibers arising from lamellipodial membrane retraction (Fig. 12*A*). We challenged macrophages with fluorescent *E. coli* particles, without prestimulation with LPS, and counted newly extended filopodia over a 20-min recording period (Fig. 12, *B–D*). Filopodia were formed by Myo10-deficient macrophages, but the total number per cell was greatly reduced compared with wild-type cells (Fig. 12*D*).

In another series of experiments, we compared the rates of filopodia formation in WT, $Myo10^{tm2/tm2}$, and Cdc42 cKO macrophages during time-lapse recordings, with or without

[3] A. C. Bachg, M. Horsthemke, B. V. Skryabin, T. Klasen, C. Faber, E. Woodham, L. M. Machesky, S. Bachg, T. Pap, S. Teufel, C. Hartmann, M. Bähler, and P. J. Hanley, unpublished data.

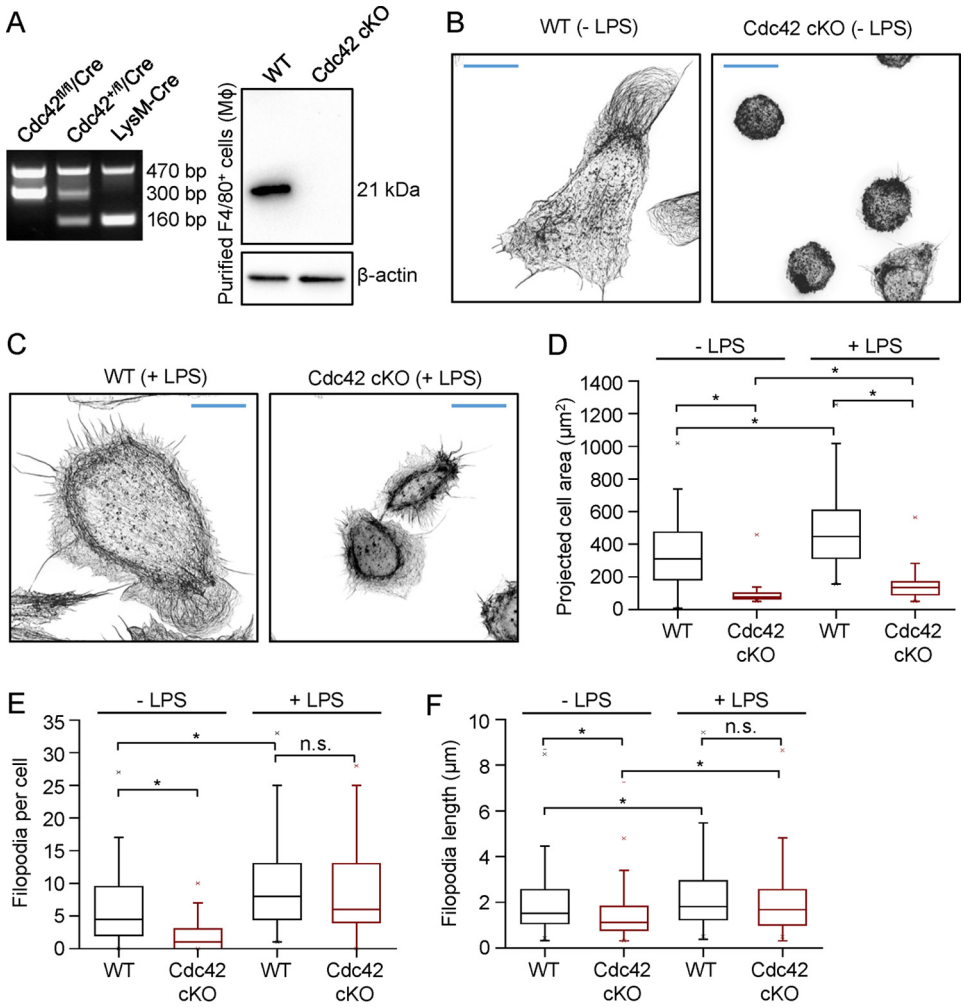

Figure 6. Phenotype of macrophages lacking the filopodia-inducing Rho GTPase Cdc42. *A*, PCR genotyping of offspring derived from intercrossing Cdc42$^{+/fl}$/LysM-Cre mice and Western blot analysis of lysates from wild-type (*WT*) and myeloid-restricted (conditional) Cdc42 knock-out (*Cdc42 cKO*; Cdc42$^{fl/fl}$/LysM-Cre) mouse peritoneal macrophages, after cell sorting for F4/80^{+} (mouse macrophage marker positive) cells. *B*, SR-SIM images of mouse resident peritoneal macrophages isolated from WT and Cdc42 cKO mice, respectively. Macrophages were fixed, permeabilized, and stained with a high-affinity F-actin probe (Alexa Fluor 488-conjugated phalloidin). *Scale bars*, 10 μm. *C*, SR-SIM images of WT and Cdc42 cKO macrophages activated by stimulation with 1 μg/ml of lipopolysaccharide (*LPS*) for 90 min. *Scale bars*, 10 μm. *D*, box plots showing the (two-dimensional projected) cell area of WT and Cdc42 cKO macrophages before and after stimulation with LPS ($n = 75–162$ cells). *E*, box plots showing the number of filopodia per cell before and after stimulation with LPS ($n = 44–96$ cells). *F*, box plots showing filopodia lengths before and after stimulation with LPS ($n = 158–644$ events). *, $p < 0.05$; Kruskal-Wallis one-way analysis of variance on ranks. *n.s.*, nonsignificant.

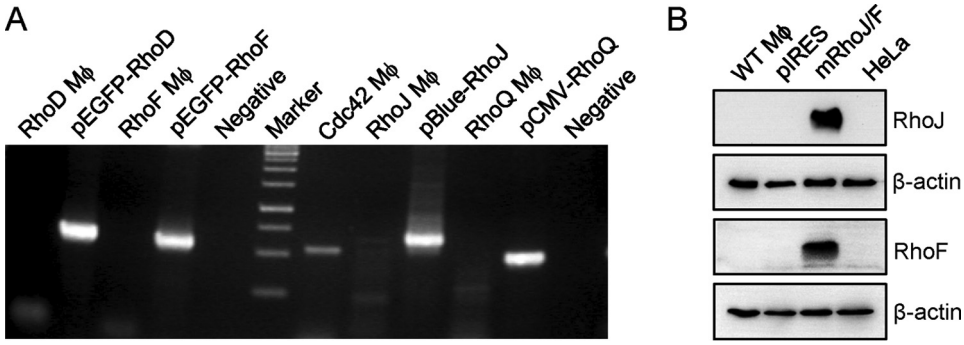

Figure 7. Expression of Cdc42, but not other filopodia-inducing Rho GTPases in mouse macrophages. *A*, RT-PCR analysis, including positive controls, of the expression pattern of filopodia-inducing Rho GTPases (RhoD, RhoF, RhoJ, and RhoQ) in mouse macrophages. *B*, Western blot analysis, including positive controls, showing no expression of RhoJ or RhoF protein in mouse macrophages.

pretreatment with LPS (1 μg/ml for 45 min) (Fig. 13, *A–D*). Consistent with the findings in Fig. 12, filopodia formation was markedly impaired in Myo10-deficient macrophages. Moreover, comparison of the images in Fig. 13, *C* (Myo10$^{tm2/tm2}$) and *D* (Cdc42 cKO), underscore the spreading defect of Cdc42-deficient macrophages (see also Fig. 6), as well as the importance of distinguishing retraction fibers from filopodial protrusions, especially in the case of Myo10-deficient cells.

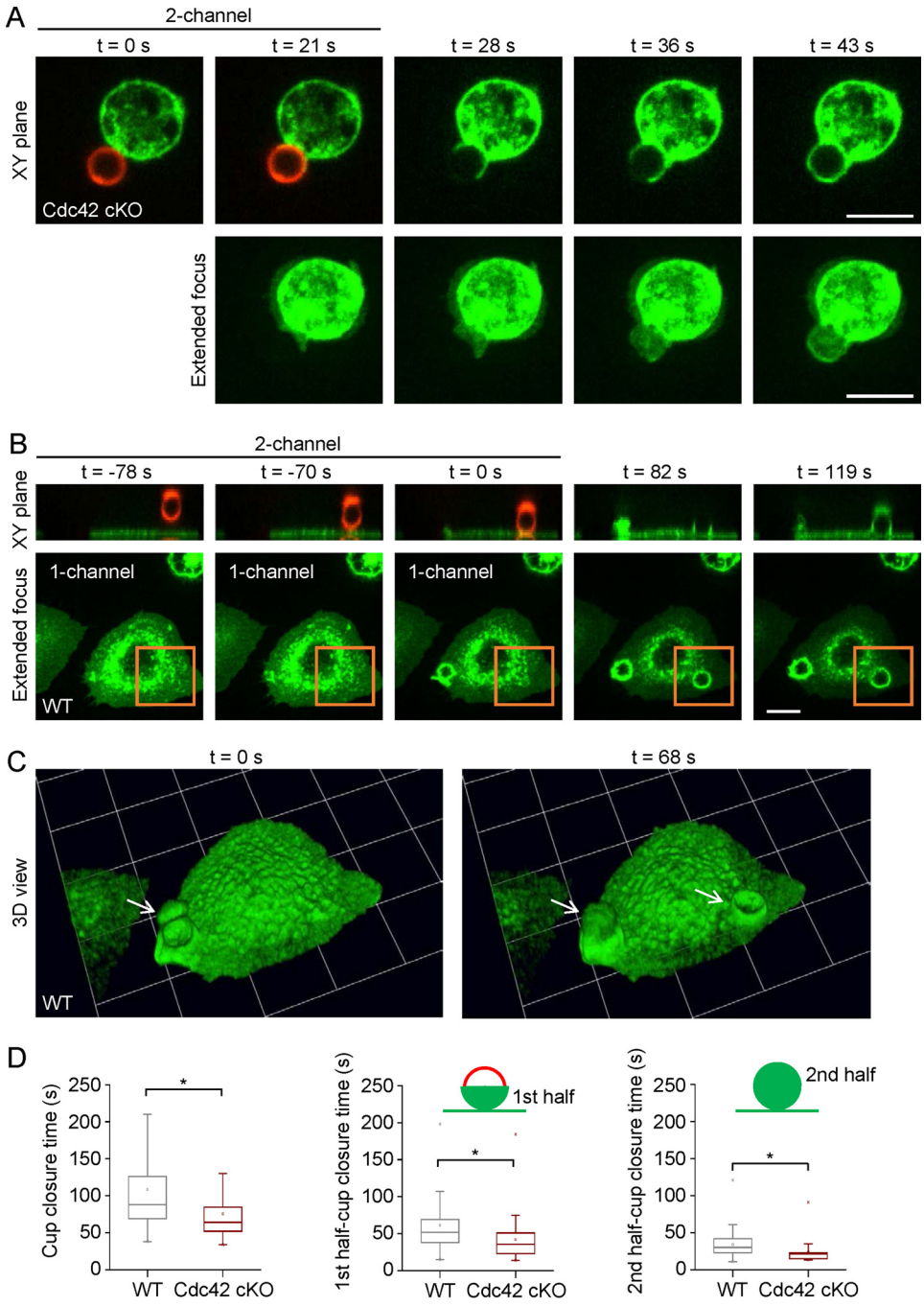

Figure 8. The kinetics of phagocytic cup formation is not impaired in Cdc42-deficient macrophages. *A*, time-lapse images, obtained by spinning disk confocal microscopy, of phagocytic cup formation by a Cdc42 cKO macrophage ingesting a mouse IgG-coated, 5.19-μm diameter polystyrene bead (labeled with Alexa Fluor 594-conjugated secondary antibodies). The macrophage was labeled with Alexa Fluor 488-conjugated anti-F4/80 antibodies. *B*, time-lapse images showing an IgG-coated polystyrene bead landing on a lamellipodium, followed by phagocytic cup formation. Macrophages were labeled with Alexa Fluor 488-conjugated anti-F4/80 antibodies. *Scale bar*, 10 μm. *C*, time-lapse three-dimensional views nicely showing phagocytic cup formation. The *white arrow* in the left image indicates an overshooting membrane extension, which subsequently flopped over the particle (*right image*). Grid spacings correspond to 12.24 μm. *D*, box plots of the time required for phagocytic cup formation, from initiation to closure, by WT ($n = 53$) and Cdc42 cKO ($n = 48$) macrophages, respectively. *, $p < 0.05$; Mann-Whitney *U* test.

Discussion

Phagocytosis, the uptake of large particles, requires the force generated by actin polymerization to drive plasma membrane extensions around a target particle and form a phagocytic cup, followed by phagosome formation (28–30). However, before a particle can be ingested it first needs to come in contact with a phagocyte. In 2010, Flannagan *et al.* (31) reported that particle-phagocytic receptor interactions were not passive, stochastic events, but, instead, macrophages continually probe the environment using Rac-dependent membrane protrusions. Filopodia, finger-like structures containing actin bundles, are highly suitable for probing the environment (2), and can be induced by "switching on" Cdc42 via Cdc42 guanine nucleotide exchange factors (22). As proof of principle, stud-

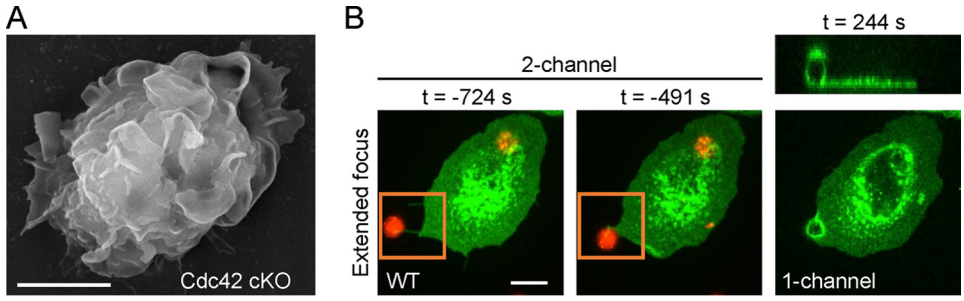

Figure 9. High-resolution image of a Cdc42-deficient (Cdc42 cKO) macrophage and filopodium-mediated capture of a large bead by a WT cell. *A*, scanning electron microscopy image of a Cdc42-deficient macrophage. *Scale bar*, 4 μm. *B*, time-lapse images showing capture of an IgG-coated polystyrene bead by a filopodium, followed by phagocytic cup formation. *Scale bar*, 10 μm.

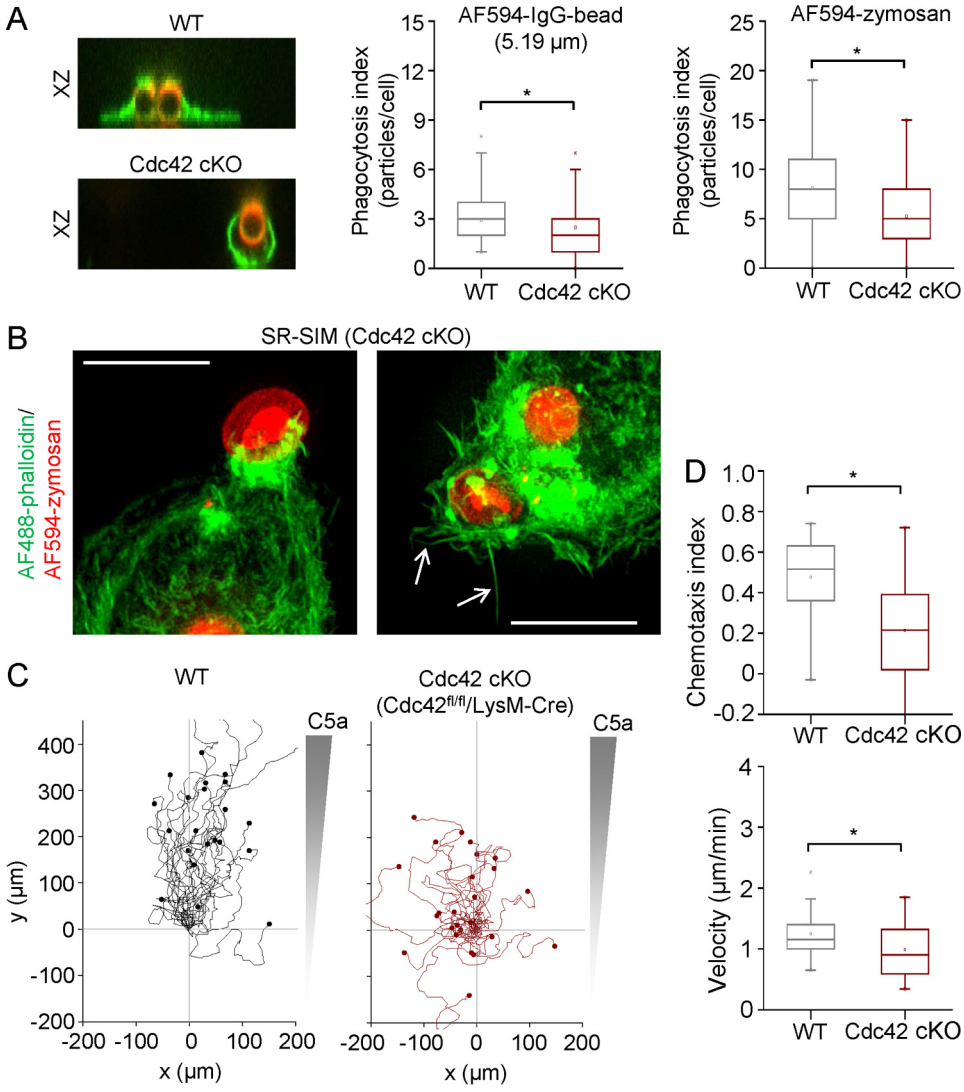

Figure 10. Impaired particle clearance and chemotactic navigation of Cdc42-deficient macrophages. *A*, end-point assays showing the number of mouse IgG-coated, 5.19-μm diameter polystyrene beads (labeled with Alexa Fluor 594-conjugated secondary antibodies) or Alexa Fluor 594-conjugated zymosan particles ingested by WT and Cdc42 cKO macrophages, respectively, after 15 min incubation, followed by wash steps. *B*, snapshots of zymosan ingestion by Cdc42 cKO macrophages showing an extending phagocytic cup (*left image*) and filopodial tentacles emerging from a closed phagocytic cup (*right image*). The *white arrows* indicate filopodia. Macrophages were fixed, permeabilized, stained with Alexa Fluor 488-conjugated phalloidin, and imaged by SR-SIM. *Scale bars*, 5 μm. *C*, migration plots of WT and Cdc42 cKO macrophages in a chemotactic complement C5a gradient. *D*, summary box plots of velocity and chemotactic efficiency (chemotaxis index). *, $p < 0.05$; Mann-Whitney *U* test ($n = 75$ each group; 3 independent experiments).

ies using optical traps (tweezers) to present microbeads to macrophages showed that filopodia can pull beads (6), or, alternatively, beads can surf along filopodia toward the cell body (32). We asked what are the roles of filopodial dynamics in practice when primary macrophages are challenged with fungal or bacterial particles? In addition, we investigated the roles of the filopodia-inducing proteins Cdc42 and Myo10 in phagocytosis.

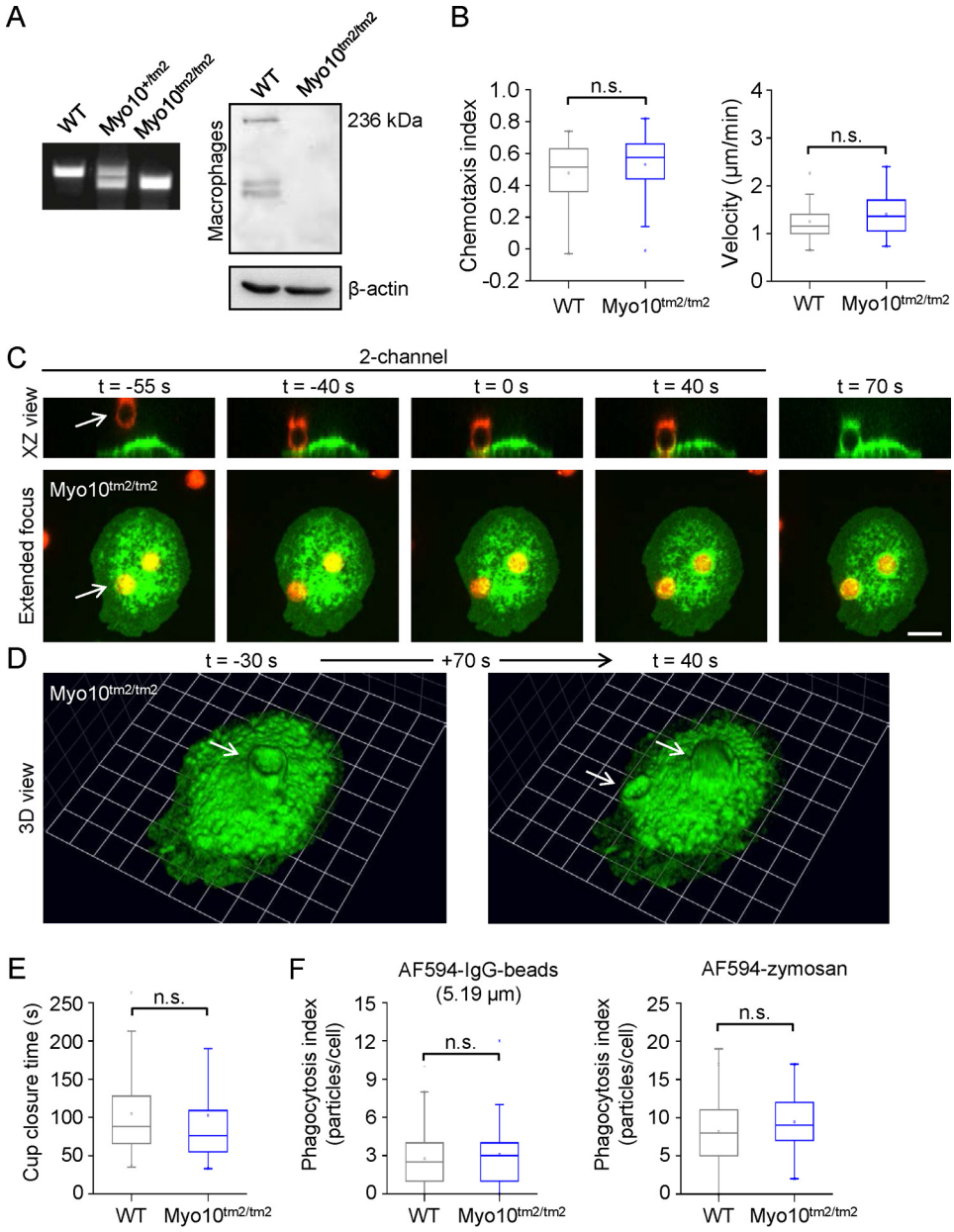

Figure 11. Myo10 is not required for phagocytic cup formation and large particle phagocytosis. *A*, PCR genotyping of offspring derived from crossing heterozygous Myo10 reporter knock-out ($Myo10^{+/tm2} \times Myo10^{+/tm2}$) mice, and Western blot analysis of Myo10 protein expression in WT *versus* homozygous Myo10 knock-out ($Myo10^{tm2/tm2}$) macrophages, purified by cell sorting. *B*, summary box plots of velocity and chemotactic efficiency (chemotaxis index). *n.s.*, not significant at a significance level of 0.05; Mann-Whitney *U* test ($n = 75$ each group; pooled WT data from Fig. 10*D*). *C*, time-lapse images showing an IgG-coated polystyrene bead landing on the cell body of a Myo10-deficient macrophage, followed by phagocytic cup formation. The macrophage was labeled with Alexa Fluor 488-conjugated anti-F4/80 antibodies. The *white arrows* correspond to the same particle. *Scale bar*, 10 μm. *D*, three-dimensional images showing phagocytic cup formation during the engulfment of the two red fluorescent particles seen in *panel C*. Grid spacings correspond to 5.07 μm. *E*, box plots of the time required for phagocytic cup formation, from initiation to closure, by WT ($n = 101$; pooled WT data from Fig. 8*D*) and Myo10-deficient ($n = 66$) macrophages, respectively. *n.s.*, not significant at a significance level of 0.05; Mann-Whitney *U* test. *F*, end-point assays showing the number of mouse IgG-coated polystyrene beads or Alexa Fluor 594-conjugated zymosan particles ingested by WT and Myo10-deficient macrophages, respectively, after 15 min incubation, followed by wash steps.

We found that resident Lifeact-EGFP macrophages could capture moderately large (~3 μm diameter) zymosan particles beyond the cell body using filopodial tentacles. Particle binding triggered the flow of actin and membrane toward the particle, rather than simple retraction, such that filopodial tentacles widened and could support phagocytic cup formation, followed by internalization and new tentacle growth. A similar outward flow of the membrane, forming a pedestal, has been observed when a zymosan particle, initially held by a micropipette, is brought into contact with a neutrophil, held by a second micropipette (33). In contrast, no membrane protrusive effect was observed when neutrophils were presented with antibody-opsonized beads (33). Zymosan is a glucan prepared from yeast (*Saccharomyces cerevisiae*) cell wall and is recognized by TLR2/TLR6 (Toll-like receptor 2/Toll-like receptor 6) heterodimers and Dectin-1 (34, 35), and possibly also mannose receptors (36). Using macrophages isolated from TLR2/TLR4 dKO, Dectin-$1^{-/-}$ and $MR^{-/-}$ mice, we confirmed that mouse macrophage

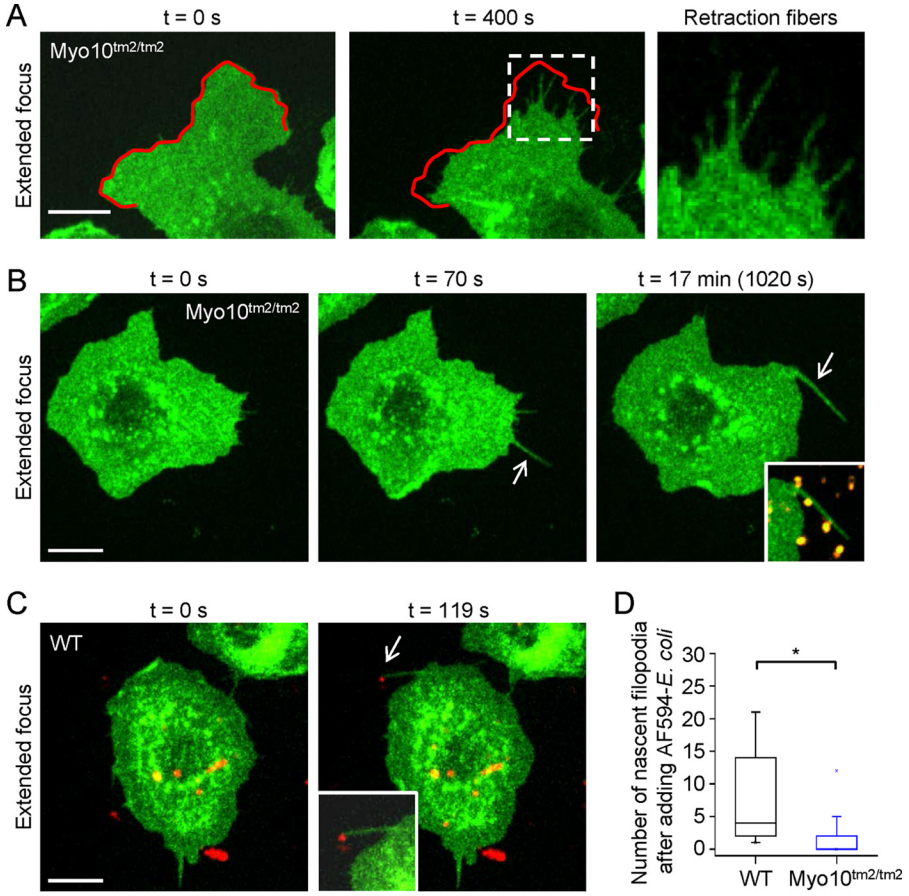

Figure 12. Deletion of Myo10 decreases nascent filopodia formation. *A*, time-lapse recording of a fluorescently labeled Myo10-deficient (Myo10$^{tm2/tm2}$) macrophage showing the appearance of retraction fibers following the retraction of a lamellipodial membrane protrusion. *Scale bar*, 10 μm. *B*, formation of *bona fide* filopodia (indicated by *white arrows*) by a Myo10-deficient macrophage challenged with *E. coli* particles (for clarity, only the *green* (membrane) channel is shown). The *inset* shows the overlay of *green* (membrane) and *red* (*E. coli* particles) channels. *C*, filopodia formation by a wild-type (WT) macrophage. *Scale bar*, 10 μm. *D*, summary box plot showing the number of nascent filopodia formed by WT ($n = 34$) *versus* Myo10 knock-out ($n = 64$) macrophages over a 20-min recording period. *, $p < 0.05$; Mann-Whitney *U* test ($n = 2$ independent experiments).

zymosan binding and phagocytosis are primarily mediated by Dectin-1. We infer that Dectin-1, akin to Fcγ-receptors, transduces phagocytic signaling through an immunoreceptor tyrosine-based activation motif-like domain (37), and evokes anterograde actin flow and phagocytic cup formation when a filopodium makes contact with a zymosan particle (see schematic diagram, Fig. 14*A*).

Filopodial tentacles were highly efficient at fishing out *E. coli* particles beyond the cell body. We observed four main mechanisms (in order of frequency): capture and surfing along the filopodium, sweeping actions, combinations of surfing and retraction, and simple retraction (see schematic summary, Fig. 14*B*). In contrast to studies using optical traps (6, 32), we did not bring particles to macrophage protrusions, but, rather, macrophages were required to seek and capture targets. Notably, time-lapse imaging was important to distinguish the formation and dynamics of filopodia from the formation of retraction fibers. On the one hand, the relative contribution of surfing to particle uptake may have been inflated because retraction fibers were variably present at the start of time-lapse recordings. On the other hand, retraction fibers are structurally related to filopodia and similarly contain parallel, bundled actin (38). Furthermore, Svitkina *et al.* (38) demonstrated using time-lapse imaging that filopodia and retraction fibers are interconvertible structures. *E. coli* particles surfed along filopodia with velocities of 1–2 μm/min, marginally slower than measured rates of retrograde flow (2–4 μm/min). Assuming that the surfing of bound particles is driven by actin retrograde flow, a mechanism linking particles to actin filaments is required. Unconventional myosins could fulfill this role, along the lines nicely illustrated in Fig. 3 of the review article by Mermall *et al.* (39), or possibly the ERM (ezrin, radixin, and moesin) protein family could play a role (40).

In the pioneering study by Nobes and Hall (22), the injection of constitutively active Cdc42, together with inhibitors of Rac and Rho, into Swiss 3T3 (embryonic fibroblast-derived) cells was shown to induce filopodial tentacles remarkably similar to those we observed in macrophages, whereas this effect was much weaker in the presence of Rac activity. It is now known that Cdc42 stimulates actin nucleation by the actin-related protein-2/3 (Arp2/3) complex via WASP (Wiskott-Aldrich syndrome protein), which is predominantly expressed in hematopoietic cells (41). The Cdc42-WASP-Arp2/3 pathway is thought to be important for the initiation of filopodia formation, but, importantly, other proteins can induce filopodia, such as RIF (RhoF), mammalian Diaphanous-like (mDia) formins, and Myo10 (2). In relationship to this point, we could not detect filopodia-inducing Rho GTPases, other than Cdc42, in macro-

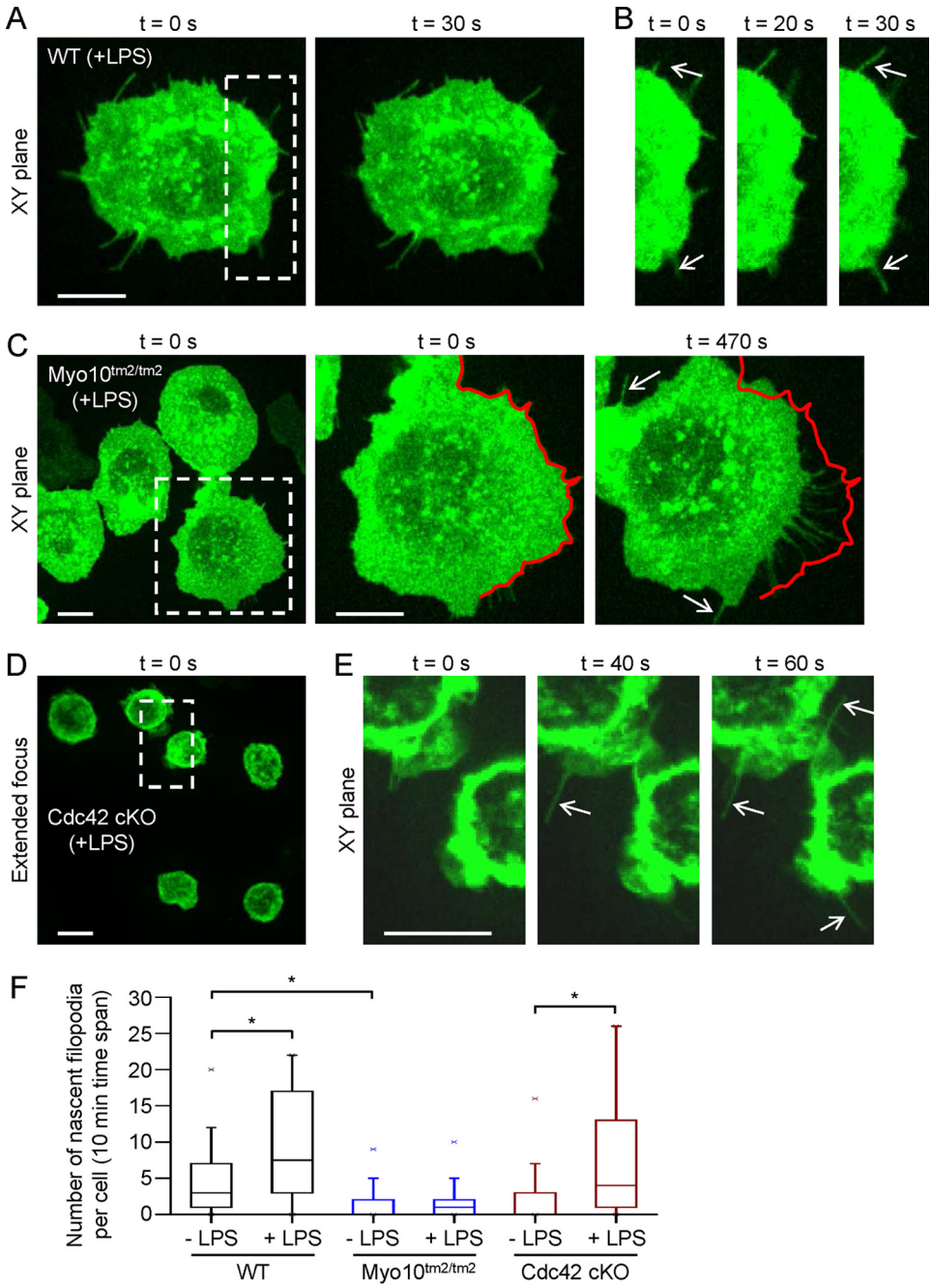

Figure 13. Paucity of nascent filopodia in Myo10 knock-out macrophages. *A*, time-lapse images of WT macrophages, prestimulated with LPS for 45 min, showing the formation of new finger-like membrane protrusions (filopodia). *Scale bar*, 10 μm. *B*, time-lapse 10 $\times$ 30-μm images cropped from the cell shown in *panel A*. Image intensity has been increased to better visualize (thin) filopodia, indicated by *white arrows*. *C*, image of four Myo10-deficient ($Myo10^{tm2/tm2}$) macrophages (*scale bar*, 10 μm) stimulated with LPS. Enlarged views of one of the cells is shown at two different time points. Note the formation of filopodia (*white arrows*) and retraction fibers (the right membrane perimeter (marked *red*) at $t = 0$ s has been superimposed on the same cell at $t = 470$ s). *D* and *E*, Cdc42 cKO macrophages (*scale bar*, 10 μm) and 15 $\times$ 25-μm cropped view (*scale bar*, 10 μm) at different time points. *White arrows* indicate filopodia. *F*, summary data showing number of new filopodia over a 10-min recording period formed by macrophages without LPS (*−LPS*) or with LPS (*+LPS*) pretreatment. *, $p < 0.05$; Kruskal-Wallis one-way analysis of variance on ranks (at the 0.05 level of significance) ($n = 30–42$ cells per group; 2 independent experiments).

phages, although mDia1, mDia2 (42), and Myo10 (Fig. 11) are expressed in macrophages.

Remarkably, macrophages from myeloid-restricted Cdc42 knock-out mice had an aberrant rounded-up morphological phenotype, which was not rescued by activation with a chemoattractant (complement C5a) or the TLR4 ligand LPS (lipopolysaccharide). This overt phenotype suggests that, at least in the case of macrophages, the Cdc42-WASP pathway, rather than the Rac-WAVE (WASP family verprolin homologs) pathway, plays a predominant role in stimulating Arp2/3 activity and lamellipodial spreading. Less surprisingly, we found that chemotactic navigation and cell velocity were decreased in Cdc42 conditional knock-out macrophages, compared with WT cells, in line with observations in neutrophils (24) and dendritic cells (25), as well as earlier work using dominant-negative constructs (26). Indeed, Yang *et al.* (43) recently showed in ele-

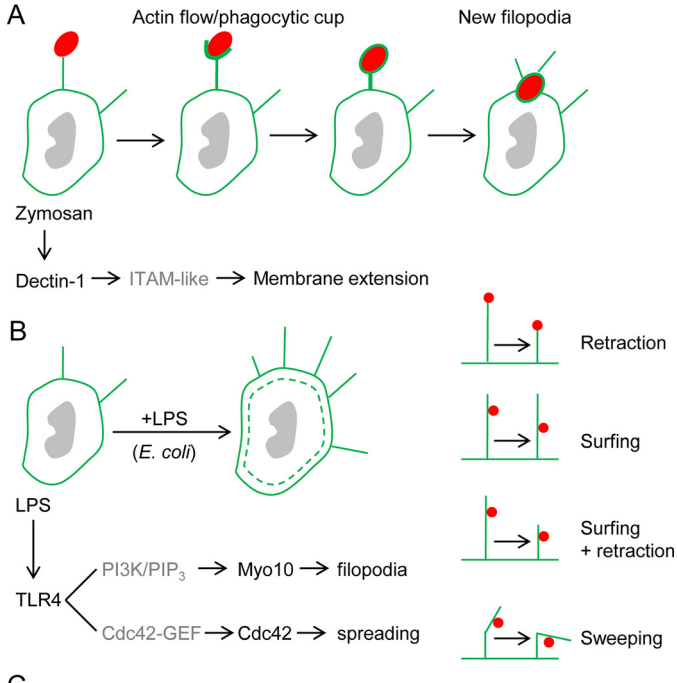

C

	2D chemotaxis	Phagocytic cup formation
Myo10	Redundant	Redundant
Cdc42	Critical	Redundant

Figure 14. Schematic summary. *A*, zymosan phagocytosis in mouse macrophages is driven by Dectin-1 receptors. When a zymosan particle is engaged by a filopodium, Dectin-1 presumably signals via its immunoreceptor tyrosine-based activation motif (*ITAM*)-like domain to induce outward actin flow and phagocytic cup formation. Following ingestion, nascent filopodia grow upon the closed phagocytic cup. *B*, the TLR4 (Toll-like receptor 4) ligand LPS (lipopolysaccharide), derived from the cell wall of Gram-negative bacteria such as *E. coli*, induces cell spreading and filopodia formation within 60 min of application. Spreading is markedly impaired in Cdc42-deficient macrophages, whereas Myo10-deficient macrophages have normal spreading, but reduced filopodia formation. Myo10 harbors pleckstrin homology domains, which promote binding to PIP_3 (phosphatidylinositol (3,4,5)-trisphosphate)-rich membranes. PIP_3 production is catalyzed by PI3K (phosphoinositide 3-kinase), activated by various pathways, including TLR4 signaling. Time-lapse imaging reveals multiple modes in which filopodia support particle capture and ingestion, including retraction of the tip-bound particle (*red spot*) toward the cell body, surfing of an attached particle along the shaft of a filopodium (presumably driven by actin retrograde flow), combinations of surfing and retraction, and sweeping actions. *C*, summary table. Both Myo10 and Cdc42 are redundant for phagocytic cup formation, whereas Cdc42, but not Myo10, is important for chemotactic navigation.

gant experiments that local activation of Cdc42, rather than Rac and Rho, chemotactically steer neutrophil-like cells. Moreover, loss of Cdc42 antagonism of RhoA, documented by Yang *et al.* (43), may explain the rounded-up phenotype we observed in Cdc42-deficient macrophages. We did not explore this possibility further, although, as proof of principle, Myo9b knock-out macrophages have both increased RhoA activity and a rounded up morphology, which is rescued by Rho inhibition (21).

Recently, knockdown of Cdc42 was reported to decrease the phagocytosis of large particles, giving rise to the notion that Cdc42 activity is required to take "big bites" (10). In contrast, we found that Cdc42-deficient macrophages generate phagocytic cups and engulf large particles (~5.19 μm diameter) at a faster rate than WT cells. The faster phagocytic cup kinetics is probably due to the highly ruffled surface geometry of (rounded-up) mutant cells, which provides a rich local source of actin and membrane. Phagocytic cup formation upon a thin lamellipodial membrane protrusion in WT cells, in comparison, requires assimilation of actin and membrane over greater distances. Unstimulated Cdc42 conditional knock-out macrophages, imaged by SR-SIM, exhibited less filopodia than WT cells, as anticipated, and, in addition, the median filopodial length was significantly less in mutant cells. However, no significant differences in the number or lengths of filopodia, Cdc42 cKO *versus* WT macrophages, were observed after stimulating cells with LPS. Thus, LPS primes macrophages for the capture of bacteria by inducing filopodia formation (Fig. 14*B*), which is not critically dependent on Cdc42 activity.

Myo10 has been implicated in phagocytosis (11, 44), but, surprisingly, we found that Myo10-deficient macrophages had no impairment in the engulfment of large IgG-opsonized beads, IgG-opsonized human red blood cells,[3] or zymosan particles. Moreover, Myo10 was redundant for cell spreading, motility, and chemotaxis. However, in further time-lapse imaging assays, we found that the frequency of filopodia formation was greatly reduced in Myo10 knock-out macrophages challenged with *E. coli* particles or LPS. Thus, Myo10 is important for the initiation of filopodia in macrophages. Importantly, as emphasized earlier, time-lapse imaging allowed filopodia to be easily distinguished from retraction fibers.

In conclusion, as partly illustrated in Fig. 14, we show that 1) zymosan engulfment is primarily mediated by Dectin-1, rather than mannose or Toll-like receptors, and in the case when a filopodium makes contact with a zymosan particle, Dectin-1 signaling triggers actin flow along the shaft toward the particle and phagocytic cup formation (Fig. 14*A*), 2) LPS, a component of Gram-negative bacteria such as *E. coli*, induces cell spreading and filopodia formation, the latter of which can help clear bacterial particles by various means: retraction, surfing, combinations of surfing and retraction, or sweeping (Fig. 14*B*), 3) both resting and LPS-induced cell spreading requires Cdc42, but not Myo10, whereas the Myo10 promotes filopodia formation in macrophages, and 4) Cdc42, but not Myo10, is important for cell motility and chemotactic navigation in a complement C5a gradient (Fig. 14*C*).

Experimental procedures

Mice

Lifeact-EGFP mice were generated as previously described by Riedl *et al.* (8). To generate myeloid-restricted Cdc42 knock-out mice, Cdc42 ($Cdc42^{fl/fl}$) mice, described by Wu *et al.* (45) and kindly supplied by Cord Brakebusch, were crossed with LysM-Cre mice (referred to as $Lyz2^{tm1(cre)Ifo}$ mice by the Mouse Genome Informatics database), kindly supplied by Irmgard Förster (Heinrich-Heine-Universität, Düsseldorf). Heterozygous Myo10 reporter knock-out ($Myo10^{+/tm2}$) mice were obtained from the Wellcome Trust Sanger Institute (Hinxton, Cambridge, United Kingdom). Phenotypic analysis of these mice is documented in Bachg *et al.*[3] TLR2 (Toll-like receptor 2) and TLR4 double mutant (TLR2/4 double knock-out) mice, described by Spiller *et al.* (46), were obtained from Carsten

Kirschning (Universität Duisburg-Essen), and mannose receptor knock-out ($MR^{-/-}$) mice were provided by Sven Burgdorf (LIMES (Life & Medical Sciences) Institut, Bonn). Dectin-1-deficient (Dectin-$1^{-/-}$) mice were kindly provided by Gordon Brown (University of Aberdeen) and Laura E. Layland (Universitätsklinikum Bonn). Mice were bred in specific pathogen-free conditions and used in accordance with local animal experimentation guidelines. All procedures were approved by the University of Münster animal care and use committee.

Genotyping

PCR for genotyping the Cdc42 conditional knock-out mouse line was performed in two phases. First, touchdown PCR was performed using the following thermocycling protocol: 94 °C for 7 min, then 10 cycles of 94 °C for 30 s, 65 to 55 °C (starting at 65 °C and subtracting 1 °C each cycle) for 30 s, and 72 °C for 45 s. This was followed by 35 cycles of 94 °C for 30 s, 55 °C for 30 s, and 72 °C for 45 s. The following primer sequences (5′ → 3′) were used: Cdc42 forward, TCTGCCATCTACACATACAC; Cdc42 reverse, ATGTAGTGTCTGTCCATTGG. The product sizes were 160 bp (wild-type allele) and 300 bp (floxed Cdc42 allele). The LysM-Cre allele was detected using the following primer pair (product size, 470 bp): forward (Cre-F), CCAATTTACTGACCGTACACC; reverse (Cre-R), TATATCCTGGCAGCGATCGC. PCR genotyping for the Lifeact-EGFP mouse line was performed using a hot start (94 °C) and the following thermocycling protocol: 35 cycles of 94 °C for 30 s, 70 °C for 30 s, and 72 °C for 60 s. The following primer sequences (5′ → 3′) were used for the Lifeact-EGFP allele (product size, 265 bp): EGFP forward, GCACGACTTCTTCAAGTCCGCCATGCC; EGFP reverse, GCGGATCTTGAAGTTCACCTTGATGCC. As positive control, a primer pair giving a 466-bp product was used: *Fabp2* (fatty acid-binding protein 2, intestinal) forward, CCTCCGGAGAGCAGCGATTAAAAGTGTCAG; *Fabp2* reverse, TAGAGCTTTGCCACATCACAGGTCATTCAG.

Antibodies

Resident peritoneal macrophages were purified by cell sorting using rat anti-mouse F4/80 antibodies conjugated to Alexa Fluor 488 (5:200 dilution; MCA497A488, AbD Serotec, Germany, or MF48020, Molecular Probes, Life Technologies). The following antibodies were used for Western blot analyses: mouse anti-Cdc42 (1:1000 dilution; catalogue number 11A11, Cell Signaling Technology), rabbit anti-RhoQ (also known as anti-TC10; 1:1000 dilution; catalogue number, PA1–1061, Thermo Fisher Scientific), mouse anti-RhoJ (used at 1 μg/ml; catalogue number, ab57584, Abcam), rabbit anti-RhoF (used at 10 μg/ml; catalogue number, ab81024, Abcam) and goat anti-RhoD (1:500 dilution; catalogue number, sc-27880, Santa Cruz Biotechnology). Mouse monoclonal anti-β-actin antibodies (clone AC-15; catalogue number, A1978, Sigma-Aldrich, Germany), diluted 1:2000, were used to control loading in Western blot analyses. The following secondary antibodies were used: horseradish peroxidase-conjugated goat anti-mouse IgG polyclonal antibodies (115-035-003; Jackson ImmunoResearch Laboratories), horseradish peroxidase-conjugated goat anti-rabbit IgG polyclonal antibodies (111-035-003; Jackson ImmunoResearch Laboratories), and horseradish peroxidase-conjugated rabbit anti-goat IgG polyclonal antibodies (sc-2922; Santa Cruz Biotechnology).

Plasmids and cloning

To generate positive controls for Western blot analyses, the coding sequences of "mouse" RhoJ, RhoQ, RhoD, and RhoF were subcloned into the expression vector pIRES2-DsRed2 (Clontech), which contains an internal ribosomal entry site (IRES) and an expression reporter (DsRed2), which encodes the red fluorescent protein DsRed2. The parent plasmids containing the genes of interest were pBluescript-RhoJ (insert accession number, AK003482; Source BioScience), pCMV6-RhoQ (insert accession number, BC056363; OriGene Technologies), pEGFP-RhoD (plasmid 23236; Addgene), and pEGFP-RhoF (gift from Harry Mellor). Successful insertion of the respective mouse Rho GTPase genes into the vector pIRES2-DsRed2 (yielding pIRES-RhoJ, pIRES-RhoQ, pIRES-RhoD, and pIRES-RhoF) was confirmed by DNA sequencing.

Isolation and handling of resident peritoneal macrophages

Mice were killed by an overdose of isoflurane in air, and the peritoneal cavity was lavaged via a 24-guage plastic catheter (B. Braun, Melsungen, Germany) using 2 × 4.5 ml of ice-cold Hank's balanced salt solution without Ca^{2+} or Mg^{2+} (Thermo Fisher Scientific). After centrifugation (300 × *g* for 6.5 min), cells were resuspended in bicarbonate-free RPMI 1640 medium containing 20 mM Hepes (Biochrom AG, Berlin, Germany), and supplemented with 10% heat-inactivated fetal calf serum (FCS), 100 units/ml of penicillin, and 100 μg/ml of streptomycin (pH 7.4). The cells were seeded into fibronectin-coated μ-slide I chambers or μ-slide chemotaxis chambers (Ibidi, Martinsried, Germany), and placed in a humidified incubator (37 °C). After 2 h, μ-slide I chambers were filled with 1 ml of RPMI 1640 medium, including 10% FCS and antibiotics, and incubated overnight at 37 °C with 5% CO_2. Experiments were performed after switching back to bicarbonate-free RPMI 1640 medium containing 20 mM Hepes. Alternatively, cells were seeded onto fibronectin-coated glass coverslips or glass bottom dishes.

Cell sorting

Mouse peritoneal macrophages were labeled with Alexa Fluor 488-conjugated anti-F4/80 antibodies, washed, and resuspended in autoMACS Running Buffer (130-091-221; Miltenyi Biotec), containing phosphate-buffered saline, 2 mM EDTA, and 0.5% bovine serum albumin (pH 7.2). Cell sorting and cell analyses were performed using a BD FACSAria II (or FACSAria III) cell sorter (BD Biosciences, San Jose, CA).

Western blot analyses

Macrophages and NIH-3T3 cells, transfected with Rho GTPase constructs, were lysed using Cell Lysis Buffer (number 9803; Cell Signaling Technology) containing: 20 mM Tris-HCl (pH 7.5), 150 mM NaCl, 1 mM Na_2EDTA, 1 mM EGTA, 1% Triton X-100, 2.5 mM sodium pyrophosphate, 1 mM β-glycerolphosphate, 1 mM Na_3VO_4 (phosphatase inhibitor), and 1 μg/ml of leupeptin (protease inhibitor), supple-

mented with 5 mM NaF (phosphatase inhibitor), 10 μg/ml of aprotinin (inhibitor of trypsin and related proteases), 10 μg/ml of Pefabloc SC (proteinase K inhibitor), and 1 mM DTT (dithiothreitol; also known as Cleland's reagent), a reducing agent. Proteins were separated by 15% SDS-PAGE and transferred onto polyvinylidene difluoride membranes (Roche Applied Science). Membranes were blocked for 1 h at room temperature in TBS containing 5% bovine serum albumin and 0.1% Tween 20 followed by overnight incubation (4 °C) with primary antibodies. For detection, horseradish peroxidase-conjugated secondary antibodies were used in combination with SuperSignal West Pico chemiluminescence substrate (Perbio, Bonn, Germany).

Two-dimensional chemotaxis assays

Cells obtained by peritoneal lavage of a single mouse were resuspended in 125–175 μl of medium, and 10 μl of the suspension was seeded into the narrow (1000 × 2000 × 70 μm) channel of an uncoated (IbiTreat) μ-slide chemotaxis chamber (Ibidi). The narrow channel (observation area) connects two 40-μl reservoirs. After 3 h, the chemotaxis chamber was filled with bicarbonate-free RPMI 1640 medium containing 10% FCS, 100 ng/ml of lipopolysaccharide and antibiotics. Next, 15 μl of medium containing chemoattractant (C5a) and 0.003% Patent Blue V (blue dye) was drawn into one of the reservoirs. The final concentration of C5a was 20 nM. The observation area was imaged by phase-contrast microscopy via a ×10 (NA 0.3) objective lens. The blue dye served as a visual indicator of gradient formation, and we have previously confirmed that it does not affect cell migration. Images were captured every 2 min for 14 h, and cell migration tracks between 6 and 12 h were analyzed with ImageJ software (National Institutes of Health) using a manual tracking plug-in and the chemotaxis and migration tool from Ibidi. Twenty-five randomly selected cells were manually tracked in each chemotaxis experiment.

Spinning disk confocal microscopy

Two- or three-dimensional time-lapse imaging of living macrophages was performed using an UltraVIEW Vox three-dimensional live cell imaging system (PerkinElmer Life Sciences, Rodgau, Germany) coupled to a Nikon Eclipse Ti inverse microscope. The system incorporated a Yokogawa (Japan) CSU-X1 spinning disk scanner, a Hamamatsu (Japan) C9100-50 EM-CCD camera (1000 × 1000 pixels), and Volocity software. Cells were imaged via a Nikon ×60 (NA 1.49) oil immersion objective lens, and the temperature was maintained at 37 °C using an Okolab all-in-one stage incubator (Okolab, Ottaviano, Italy). Z-stacks of Lifeact-EGFP macrophages or cells labeled with Alexa Fluor 488-conjugated anti-F4/80 antibodies were obtained using steps in the range 0.5 to 1 μm. Focal drift was circumvented using the Nikon Perfect Focus System, which tracks the position of the coverslip in the *z* axis by reflecting infrared light (870 nm) from the coverslip and detecting it via a CCD (charge-coupled device) sensor.

DIC and fluorescence imaging

In selected experiments, time-lapse DIC and fluorescence microscopy was performed using a Zeiss inverted microscope (AxioObserver) equipped with a temperature-controlled incubator (incubator XL S, Zeiss) and controlled by AxioVision software (Zeiss). Images were captured via a ×63 (NA 1.4) oil-immersion objective lens and charge-coupled device camera (AxioCam MRm, Zeiss).

Phagocytosis assays

Time-lapse imaging of phagocytic events was performed after introducing particles to macrophages seeded in fibronectin-coated μ-slide I chambers, which have a channel volume of 100 μl. Stock solutions of BioParticles (Thermo Fisher Scientific) were prepared at 20 mg/ml in Dulbecco's PBS and diluted 1:75 in live cell imaging medium, which consisted of bicarbonate-free RPMI 1640 medium containing 20 mM Hepes and 1 mM *N*-(2-mercaptopropionyl)glycine, a free radical scavenger. The suspension of BioParticles in live cell imaging medium was sonicated to disperse the particles, and 100 μl was pipetted into a μ-slide I chamber before starting time-lapse imaging via spinning disk confocal microscopy. The following BioParticles were used: Alexa Fluor 594-conjugated *E. coli* (K-12 strain) particles (E23370; Thermo Fisher Scientific), Alexa Fluor 594-conjugated zymosan (polysaccharide prepared from the cell wall of *S. cerevisiae* (bakers' yeast), catalogue number Z23374; Thermo Fisher Scientific) and pHrodo-conjugated zymosan, prepared using unlabeled zymosan (Z2849; Thermo Fisher Scientific) and the succinimidyl ester of pHrodo red (P36600; Thermo Fisher Scientific), which has absorbance and emission maxima of 560 and 585 nm, respectively. In addition, phagocytosis assays were performed using mouse IgG-coated polystyrene particles (MsGPX-50-5; Spherotech), which had a mean diameter of 5.19 μm. The 0.5% (w/v) stock solution was diluted 1:10 before use, and the beads were rendered red fluorescent by incubation with Alexa Fluor 594-conjugated goat anti-mouse IgG antibodies (ab150116; Abcam), followed by a wash step.

Scanning electron microscopy

Macrophages, seeded on fibronectin-coated glass coverslips, were fixed for 40 min with ice-cold Hepes-buffered (pH 7) medium containing 2% paraformaldehyde and 2.5% glutaraldehyde. As a pre-critical drying step, the cells were dehydrated by exposure, each time 15 min, to increasing concentrations of ethanol (30, 50, 70, 90, and 100%). The transitional fluid ethanol was replaced with liquid CO_2 and the sample was brought to a critical point for CO_2 (31 °C and 73.8 bar). Critical point drying (to remove CO_2) was achieved by subsequently decreasing the pressure at constant temperature (31 °C). The dried sample was sputter coated with platinum and imaged using an Hitachi S5000 scanning electron microscope.

Superresolution structured illumination microscopy

Superresolution-structured illumination microscopy was performed using an Elyra S.1 inverted microscope system (Carl Zeiss MicroImaging, Germany), controlled by ZEN 2011 SP2 software (black edition; Zeiss). Cells, seeded on mouse fibronectin-coated coverslips or glass bottom dishes, were imaged via an oil-immersion Plan Apo ×63 (NA 1.4) objective lens and images were captured with an Andor iXon EM-CCD. The following lasers and filters (in parentheses) were used: 488

nm (BP 495–550 nm + LP 750 nm) and 561 nm (BP 570–620 nm + LP 750 nm). Five grating positions and 5 phase shifts were used for each *z*-slice.

Statistics

Normality and homoscedasticity were tested using the Shapiro-Wilk and Levene tests, respectively. A one-way analysis of variance was used to test for statistical differences at the 0.05 level of significance. When the assumed conditions of normality and homogeneity of variance were not fulfilled, as in most cases, we used the non-parametric Mann-Whitney *U* test or Kruskal-Wallis one-way analysis of variance on ranks (at the 0.05 level of significance). Post hoc multiple comparisons were made using Dunn's method. Statistical analyses were performed using SigmaPlot (version 12) software (Systat Software), SPSS Statistics 22 (IBM Corporation), or Origin 2015 SR2 (OriginLab), and data are presented as box plots or mean ± S.E.

Author contributions—M. H., A. C. B., R. W.-S., M. S., S. T., M. B., and P. J. H. designed experiments. M. H., A. C. B., K. G., S. M., B. M., S. H., S. T., and P. J. H. performed research and analyzed data. P. J. H. wrote the paper.

Acknowledgments—We are grateful to Christiane Rasch and Ulrike Keller for processing the electron microscopy samples.

References

1. Flannagan, R. S., Jaumouillé, V., and Grinstein, S. (2012) The cell biology of phagocytosis. *Annu. Rev. Pathol.* **7,** 61–98
2. Mattila, P. K., and Lappalainen, P. (2008) Filopodia: molecular architecture and cellular functions. *Nat. Rev. Mol. Cell Biol.* **9,** 446–454
3. Metschnikoff, E. (1902) *Immunität bei Infektionskrankheiten*, Gustav Fischer, Jena
4. Young, V. B., Falkow, S., and Schoolnik, G. K. (1992) The invasin protein of Yersinia enterocolitica: internalization of invasin-bearing bacteria by eukaryotic cells is associated with reorganization of the cytoskeleton. *J. Cell Biol.* **116,** 197–207
5. Vonna, L., Wiedemann, A., Aepfelbacher, M., and Sackmann, E. (2007) Micromechanics of filopodia mediated capture of pathogens by macrophages. *Eur. Biophys. J.* **36,** 145–151
6. Kress, H., Stelzer, E. H., Holzer, D., Buss, F., Griffiths, G., and Rohrbach, A. (2007) Filopodia act as phagocytic tentacles and pull with discrete steps and a load-dependent velocity. *Proc. Natl. Acad. Sci. U.S.A.* **104,** 11633–11638
7. Möller, J., Lühmann, T., Chabria, M., Hall, H., and Vogel, V. (2013) Macrophages lift off surface-bound bacteria using a filopodium-lamellipodium hook-and-shovel mechanism. *Sci. Rep.* **3,** 2884
8. Riedl, J., Flynn, K. C., Raducanu, A., Gärtner, F., Beck, G., Bösl, M., Bradke, F., Massberg, S., Aszodi, A., Sixt, M., and Wedlich-Söldner, R. (2010) Lifeact mice for studying F-actin dynamics. *Nat. Methods* **7,** 168–169
9. Riedl, J., Crevenna, A. H., Kessenbrock, K., Yu, J. H., Neukirchen, D., Bista, M., Bradke, F., Jenne, D., Holak, T. A., Werb, Z., Sixt, M., and Wedlich-Soldner, R. (2008) Lifeact: a versatile marker to visualize F-actin. *Nat. Methods* **5,** 605–607
10. Mohammadi, S., and Isberg, R. R. (2013) Cdc42 interacts with the exocyst complex to promote phagocytosis. *J. Cell Biol.* **200,** 81–93
11. Cox, D., Berg, J. S., Cammer, M., Chinegwundoh, J. O., Dale, B. M., Cheney, R. E., and Greenberg, S. (2002) Myosin X is a downstream effector of PI(3)K during phagocytosis. *Nat. Cell Biol.* **4,** 469–477
12. Faust, N., Varas, F., Kelly, L. M., Heck, S., and Graf, T. (2000) Insertion of enhanced green fluorescent protein into the lysozyme gene creates mice with green fluorescent granulocytes and macrophages. *Blood* **96,** 719–726
13. Chhabra, E. S., and Higgs, H. N. (2007) The many faces of actin: matching assembly factors with cellular structures. *Nat. Cell Biol.* **9,** 1110–1121
14. Xu, K., Babcock, H. P., and Zhuang, X. (2012) Dual-objective STORM reveals three-dimensional filament organization in the actin cytoskeleton. *Nat. Methods* **9,** 185–188
15. Brown, G. D., Taylor, P. R., Reid, D. M., Willment, J. A., Williams, D. L., Martinez-Pomares, L., Wong, S. Y., and Gordon, S. (2002) Dectin-1 is a major β-glucan receptor on macrophages. *J. Exp. Med.* **196,** 407–412
16. Underhill, D. M., Ozinsky, A., Hajjar, A. M., Stevens, A., Wilson, C. B., Bassetti, M., and Aderem, A. (1999) The Toll-like receptor 2 is recruited to macrophage phagosomes and discriminates between pathogens. *Nature* **401,** 811–815
17. Sung, S. S., Nelson, R. S., and Silverstein, S. C. (1983) Yeast mannans inhibit binding and phagocytosis of zymosan by mouse peritoneal macrophages. *J. Cell Biol.* **96,** 160–166
18. Speert, D. P., and Silverstein, S. C. (1985) Phagocytosis of unopsonized zymosan by human monocyte-derived macrophages: maturation and inhibition by mannan. *J. Leukocyte Biol.* **38,** 655–658
19. Plestant, C., Strale, P. O., Seddiki, R., Nguyen, E., Ladoux, B., and Mège, R. M. (2014) Adhesive interactions of N-cadherin limit the recruitment of microtubules to cell-cell contacts through organization of actomyosin. *J. Cell Sci.* **127,** 1660–1671
20. Schulte, C., Ferraris, G. M., Oldani, A., Galluzzi, M., Podestà, A., Puricelli, L., de Lorenzi, V., Lenardi, C., Milani, P., and Sidenius, N. (2016) Lamellipodial tension, not integrin/ligand binding, is the crucial factor to realise integrin activation and cell migration. *Eur. J. Cell Biol.* **95,** 1–14
21. Hanley, P. J., Xu, Y., Kronlage, M., Grobe, K., Schön, P., Song, J., Sorokin, L., Schwab, A., and Bähler, M. (2010) Motorized RhoGAP myosin IXb (Myo9b) controls cell shape and motility. *Proc. Natl. Acad. Sci. U.S.A.* **107,** 12145–12150
22. Nobes, C. D., and Hall, A. (1995) Rho, rac, and cdc42 GTPases regulate the assembly of multimolecular focal complexes associated with actin stress fibers, lamellipodia, and filopodia. *Cell* **81,** 53–62
23. Massol, P., Montcourrier, P., Guillemot, J. C., and Chavrier, P. (1998) Fc receptor-mediated phagocytosis requires CDC42 and Rac1. *EMBO J.* **17,** 6219–6229
24. Szczur, K., Zheng, Y., and Filippi, M. D. (2009) The small Rho GTPase Cdc42 regulates neutrophil polarity via CD11b integrin signaling. *Blood* **114,** 4527–4537
25. Lämmermann, T., Renkawitz, J., Wu, X., Hirsch, K., Brakebusch, C., and Sixt, M. (2009) Cdc42-dependent leading edge coordination is essential for interstitial dendritic cell migration. *Blood* **113,** 5703–5710
26. Allen, W. E., Zicha, D., Ridley, A. J., and Jones, G. E. (1998) A role for Cdc42 in macrophage chemotaxis. *J. Cell Biol.* **141,** 1147–1157
27. Bohil, A. B., Robertson, B. W., and Cheney, R. E. (2006) Myosin-X is a molecular motor that functions in filopodia formation. *Proc. Natl. Acad. Sci. U.S.A.* **103,** 12411–12416
28. Swanson, J. A. (2008) Shaping cups into phagosomes and macropinosomes. *Nat. Rev. Mol. Cell Biol.* **9,** 639–649
29. Freeman, S. A., and Grinstein, S. (2014) Phagocytosis: receptors, signal integration, and the cytoskeleton. *Immunol. Rev.* **262,** 193–215
30. Kinchen, J. M., and Ravichandran, K. S. (2008) Phagosome maturation: going through the acid test. *Nat. Rev. Mol. Cell Biol.* **9,** 781–795
31. Flannagan, R. S., Harrison, R. E., Yip, C. M., Jaqaman, K., and Grinstein, S. (2010) Dynamic macrophage "probing" is required for the efficient capture of phagocytic targets. *J. Cell Biol.* **191,** 1205–1218
32. Kohler, F., and Rohrbach, A. (2015) Surfing along filopodia: a particle transport revealed by molecular-scale fluctuation analyses. *Biophys. J.* **108,** 2114–2125
33. Lee, C. Y., Herant, M., and Heinrich, V. (2011) Target-specific mechanics of phagocytosis: protrusive neutrophil response to zymosan differs from the uptake of antibody-tagged pathogens. *J. Cell Sci.* **124,** 1106–1114
34. Roeder, A., Kirschning, C. J., Rupec, R. A., Schaller, M., Weindl, G., and Korting, H. C. (2004) Toll-like receptors as key mediators in innate antifungal immunity. *Med. Mycol.* **42,** 485–498

35. Taylor, P. R., Tsoni, S. V., Willment, J. A., Dennehy, K. M., Rosas, M., Findon, H., Haynes, K., Steele, C., Botto, M., Gordon, S., and Brown, G. D. (2007) Dectin-1 is required for β-glucan recognition and control of fungal infection. *Nat. Immunol.* **8,** 31–38
36. Astarie-Dequeker, C., N'Diaye, E. N., Le Cabec, V., Rittig, M. G., Prandi, J., and Maridonneau-Parini, I. (1999) The mannose receptor mediates uptake of pathogenic and nonpathogenic mycobacteria and bypasses bactericidal responses in human macrophages. *Infect. Immun.* **67,** 469–477
37. Saijo, S., and Iwakura, Y. (2011) Dectin-1 and Dectin-2 in innate immunity against fungi. *Int. Immunol.* **23,** 467–472
38. Svitkina, T. M., Bulanova, E. A., Chaga, O. Y., Vignjevic, D. M., Kojima, S., Vasiliev, J. M., and Borisy, G. G. (2003) Mechanism of filopodia initiation by reorganization of a dendritic network. *J. Cell Biol.* **160,** 409–421
39. Mermall, V., Post, P. L., and Mooseker, M. S. (1998) Unconventional myosins in cell movement, membrane traffic, and signal transduction. *Science* **279,** 527–533
40. Niggli, V., and Rossy, J. (2008) Ezrin/radixin/moesin: versatile controllers of signaling molecules and of the cortical cytoskeleton. *Int. J. Biochem. Cell Biol.* **40,** 344–349
41. Millard, T. H., Sharp, S. J., and Machesky, L. M. (2004) Signalling to actin assembly via the WASP (Wiskott-Aldrich syndrome protein)-family proteins and the Arp2/3 complex. *Biochem. J.* **380,** 1–17
42. Colucci-Guyon, E., Niedergang, F., Wallar, B. J., Peng, J., Alberts, A. S., and Chavrier, P. (2005) A role for mammalian diaphanous-related formins in complement receptor (CR3)-mediated phagocytosis in macrophages. *Curr. Biol.* **15,** 2007–2012
43. Yang, H. W., Collins, S. R., and Meyer, T. (2016) Locally excitable Cdc42 signals steer cells during chemotaxis. *Nat. Cell Biol.* **18,** 191–201
44. Chavrier, P. (2002) May the force be with you: myosin-X in phagocytosis. *Nat. Cell Biol.* **4,** E169–E171
45. Wu, X., Quondamatteo, F., Lefever, T., Czuchra, A., Meyer, H., Chrostek, A., Paus, R., Langbein, L., and Brakebusch, C. (2006) Cdc42 controls progenitor cell differentiation and beta-catenin turnover in skin. *Genes Dev.* **20,** 571–585
46. Spiller, S., Dreher, S., Meng, G., Grabiec, A., Thomas, W., Hartung, T., Pfeffer, K., Hochrein, H., Brade, H., Bessler, W., Wagner, H., and Kirschning, C. J. (2007) Cellular recognition of trimyristoylated peptide or enterobacterial lipopolysaccharide via both TLR2 and TLR4. *J. Biol. Chem.* **282,** 13190–13198

Multiple roles of filopodial dynamics in particle capture and phagocytosis and phenotypes of Cdc42 and Myo10 deletion

Markus Horsthemke, Anne C. Bachg, Katharina Groll, Sven Moyzio, Barbara Müther, Sandra A. Hemkemeyer, Roland Wedlich-Söldner, Michael Sixt, Sebastian Tacke, Martin Bähler and Peter J. Hanley

J. Biol. Chem. 2017, 292:7258-7273.
doi: 10.1074/jbc.M116.766923 originally published online March 13, 2017